

Article

Combustion Characterisation of Bituminous Coal and Pinus Sawdust Blends by Use of Thermo-Gravimetric Analysis

Garikai T. Marangwanda ^{1,2}, Daniel M. Madyira ^{1,*}, Patrick G. Ndungu ³ and Chido H. Chihobo ²

¹ Department of Mechanical Engineering Science, University of Johannesburg, Johannesburg 2028, South Africa; gmarangwanda@gmail.com

² Department of Fuels and Energy Engineering, School of Engineering Sciences and Technologies, Chinhoyi University of Technology, Chinhoyi, Zimbabwe; chihobo@gmail.com

³ Energy, Sensors and Multifunctional Nanomaterials Research Group, Department of Chemical Sciences, Doornfontein Campus, University of Johannesburg, Johannesburg 2028, South Africa; pndungu@uj.ac.za

* Correspondence: dmadyira@uj.ac.za; Tel.: +27-76-029-8563

Abstract: The cocombustion of coal and pinus sawdust waste is an economically viable and sustainable option for increasing the share of biomass in energy production. This technology also has the potential to reduce the emission of greenhouse gases from existing coal fired power plants. The thermal synergistic effects of cocombusting Hwange bituminous coal (HC) with Pinus sawdust (PS) were thus investigated using thermogravimetric analysis. Fuel blending mass ratios of 100HC, 90HC10PS, 80HC20PS, 70HC30PS, and 100PS under an oxidative atmosphere at three different heating rates of 5, 12.5, and 20 °C/min were used for the experimental setup. Zero to negative synergy was generally observed for the mass loss curves (TG) at different blending ratios. Generally positive synergy was observed with relation to rate of mass loss curves (DTG) for the 80HC20PS and 70HC30PS fuel blends only. The ignition index increased with blending ratio by an average of 42.86%, whilst the burnout index showed a maximum increase of 14.6% at 20 °C/min. However, the combustion index representative of stability showed a decreasing trend generally for all the heating rates. No combustion index produced a linear variation with temperature, though upon evaluation, an optimum mass ratio of 20% pinus sawdust was suggested. The chosen optimum blending ratio demonstrated increased ignition and burnout indexes whilst maintaining the stability of combustion at a reasonable range.

Keywords: coal; biomass; cocombustion; thermogravimetric analysis; ignition index; burnout index; combustion index



Citation: Marangwanda, G.T.; Madyira, D.M.; Ndungu, P.G.; Chihobo, C.H. Combustion Characterisation of Bituminous Coal and Pinus Sawdust Blends by Use of Thermo-Gravimetric Analysis. *Energies* **2021**, *14*, 7547. <https://doi.org/10.3390/en14227547>

Academic Editor: Osvalda Senneca

Received: 15 September 2021

Accepted: 15 October 2021

Published: 11 November 2021

Publisher's Note: MDPI stays neutral with regard to jurisdictional claims in published maps and institutional affiliations.



Copyright: © 2021 by the authors. Licensee MDPI, Basel, Switzerland. This article is an open access article distributed under the terms and conditions of the Creative Commons Attribution (CC BY) license (<https://creativecommons.org/licenses/by/4.0/>).

1. Introduction

The timber industry in Zimbabwe is reported to be generating over 750 kilotons of sawmill waste each year, which possesses an energy potential of around 232 kilotons of oil equivalent [1]. This translates to about 15.84 kg of oil equivalent per capita against a requirement of 845 kg of oil equivalent per capita according to World bank data [2]. Zimbabwe's timber industry is mainly based on planted forestry, which is situated along the Eastern highlands within the Manicaland Province. The cool temperatures, high rainfall, and high altitudes make Manicaland ideal for growing these exotic timber species [3]. Surveys showed that the Eastern Highlands plantations cover about 0.02% of the total Zimbabwean land area and the main species within these plantations are 81,000 ha of pine, 24,000 ha of eucalyptus, and 13,000 ha wattle. Of interest to this study, pine plantations are comprised mainly of the *Pinus Taeda* and *Pinus Patula* species hence found in most of the sawmills dotted across the province [4]. On a regional level, surveys showed how large timber mills only utilize 10% of the sawdust for their process boilers and lumber drying kilns, leaving the remainder to be stockpiled [3,5]. Eventually these sawdust waste stockpiles end up decomposing or in most cases succumbing to spontaneous combustion,

which are generally considered as extreme forms of environmental pollution or hazards [3]. Hence, the exploitation of biomass waste generated by the timber industry in the Eastern highlands of Zimbabwe is necessary for obvious economic and environmental reasons.

Zimbabwean coal reserves are estimated to be over 30 billion tons, with exploitation hovering around 3 million tons a year for all the collieries combined. Hwange Colliery, Makomo Resources and Zambezi Gas are the main producers of coal and the Mid Zambezi basin located northwest of Zimbabwe, which is part of the Karoo system, plays host to the most exploited coal reserves within the country [6]. Thermal-grade coal used for powerplants across the region is usually classified as low-grade bituminous coal with a lower calorific value of 25.43 MJ/kg [7]. Unfortunately, clean coal technologies were not harnessed to help reduce the carbon footprint from coal exploitation within the region. Convectional coal combustion on its own is known to produce undesired products in large quantities, such as carbon dioxide, nitrogen oxides, sulfur oxides, and particulate matter [8]. As such, cocombustion of coal and biomass waste offers a combined approach to emission reduction and combustion efficiency improvement for boilers. Applications of cocombustion are generally skewed towards developed countries. A Combined Heat Power (CHP) plant, Amager, situated in Denmark, which was traditionally considered a coal fired plant, was successfully retrofitted to accommodate more than 50% on mass basis of biomass [9]. Various generating stations within the United States were also retrofitted to accommodate biomass, mainly wood waste, at different blending ratios, either through direct or indirect co-firing. Of particular importance is a 469 MW_e large station fitted with Cyclone boilers located within Michigan City capable of handling cofired biomass and coal, justifying applicability of this technology on a large scale [10]. China also demonstrated applicability of cofiring between coal and various biomass wastes such as Municipal Solid Wastes and even agricultural residues with different kinds of boilers with varied success [11]. Finland's FORTUM's Naantali-3 315 MW_e CHP plant experiences with cofiring emphasized the need to have an efficient fuel handling and feeding system that ensures maximum homogeneity between coal and biomass for maximum benefits [12]. Some industrial tests have even gone further to employ cocombustion of biomass and coal under oxy fuel (CO₂ and O₂ as oxidant) conditions, achieving a reduction of 120% in CO₂ emissions [13].

However, before employing cocombustion on a large scale, important experimental tests related to combustion have to be carried out. Table 1 summarizes scenarios where cocombustion was investigated experimentally by use of thermogravimetric analysis.

Table 1. Examples of coal and biomass cocombustion analysis by use of thermogravimetry.

Fuel	Experimental Method				
	Biomass blending ratios (% biomass substitution)	Max temperature (°C)	Heating rate (°C/min)	Sample mass (mg)	Purge gas
Coal fines and microalgae biomass [14]	5, 10, 15, 20	650	10	5	Air at 50 mL/min
Sub-bituminous coal and microalgae biomass [15]	30, 50, 70	900	10, 20, 40	10	Air at 100 mL/min
Low rank coal and tobacco stalk biomass [11]	50, 60, 70, 80, 90	950	10, 20, 30	500	21% pure oxygen and 79% pure nitrogen at 1 L/min
Coal and corn stalks biomass [16]	25, 50, 75	850	10, 20, 30, 40, 60	20	80% pure argon and 20% pure nitrogen at 100 mL/min
Bituminous coal, anthracite and carbonaceous wastes [17]	various	800	10, 20, 30	10	Air at 100 mL/min

Table 1. Cont.

Fuel	Experimental Method				
Coal and wheat straw biomass [18]	5, 10, 15, ... ,85, 90	1300	20	100	80% pure nitrogen and 20% pure oxygen 0.05 m ³ /h
Bituminous coal, corn stalk and sawdust biomass [19]	10, 20, 30, 50	1000	15, 60	100	Air at 100 mL/min
Coal and cellulose biomass [20]	25, 50, 75	850	10, 20, 40	10	Argon at 60 mL/min
Coal and wood chips [21]	various	1000	10, 20, 30, 40, 50	9	Air at 100 mL/min Air at 100 mL/min & pure oxygen pure nitrogen
Coal and wet sludge [22]	3, 5, 10	1300	10, 25, 40	25	pure oxygen pure nitrogen
Coal, biochar, Municipal Solid Waste, sawdust [23]	various	800	5	7	Air at 100 mL/min

Riaza et al. [24] demonstrated during their studies that NO_x emissions are reduced significantly whilst SO_x emissions are generally dependent on the biomass species being used. Similar studies by Zhou et al. [19] also demonstrated a decrease in emissions for both NO_x and SO_x when coal was cocombusted with corn stalk or sawdust. Several authors also reported NO_x reduction, with Akhtar et al. [25] pointing out how the volatiles released at low temperatures for biomass combustion are responsible for the reduction in NO_x emissions. This is because the overall combustion temperatures are lower as compared to that of coal combustion, thus theoretically, thermal NO_x is reduced [26]. In as much as cocombustion of coal and biomass generally results in NO_x reduction and SO_x reduction, power plant operators are also concerned about the variation in combustion parameters such as ignition and burnout indexes [27]. Since blending of biomass and coal results in synergy of combustion parameters, it is very important to deduce if the synergy is positive or negative. Boumanchar et al. [23] concluded that cocombustion of biomass and coal is a positive synergy process, whilst Xing et al. [28] recorded negative effects at lower temperature ranges and positive effects at higher temperature ranges. The discrepancy is caused by the different methods authors use when they want to represent synergy as a numerical value. Unfortunately, deduction of cocombustion synergy has no standardized equation which tends to result in various interpretations dependent on the combustion parameter under investigation [29–31]. However, what is common amongst TG experimental findings for cocombustion is the existence of interaction between the biomass and coal characteristics.

As highlighted in Table 1, fuel blending ratios are amongst the most common variables researchers tend to investigate. Optimization of fuel blending ratios is very important to combustion engineers for improved process results. The synergy of biomass and coal characteristics rarely results in linear variation of combustion parameters, hence the need to perform extensive experimental work coupled with good modelling techniques. As such, this research looks at the experimental methods and novel modeling techniques applicable to the cocombustion of Hwange coal and Pinus sawdust blends [32,33]. The results obtained from this research will help plug the technical hurdles that hindered integration of large-scale cocombustion of Hwange coal and Pinus sawdust. With the shared coal and pinus sawdust characteristics, this research has the potential to be used as a technical advisory document across the region as well [34]. As of 2021, various renewable energy policies were proposed by regional countries within Sub-Saharan Africa. Of interest is the support all these policies have towards greener fuels and diversification of the energy portfolio [35,36]. In summary, this research was aimed at evaluating the thermal characteristics obtained when coal from Hwange and Pinus sawdust are cocombusted in a thermogravimetric analyzer.

2. Materials and Methods

2.1. Sample Preparation

The fuel samples were prepared according to the ISO18283:2006 standard. The coal used was classified as bituminous and of thermal grade, whilst the pinus sawdust was classified under the Pinus Taeda and Patula species. All fuel samples were oven-dried at approximately 105 °C over a period of 24 h, and hence, sample grindability increased and all subsequent analysis were performed on a dry basis. The coal samples were then ground using a lab scale closed Ball Mill whilst the Pinus sawdust waste material was ground using an IKA MF 10 cutting mill. After grinding and cutting the fuel samples, manual sieves based on the ISO 3310-1 standard were used to perform sieve analysis. Using a scale with a repeatability of ± 0.6 mg for weights in the range of 2–10 mg, fuel blends were prepared according to the stipulated weight ratios and labelled accordingly. In total, 5 fuel samples were prepared for analysis: 100HC, 90HC10PS, 80HC20PS, 70HC30PS, and 100PS, with the number representing the percentage mass of the individual fuel, e.g., 90HC10PS meant 90% by mass of Hwange Coal and 10% by mass of Pinus Sawdust. Homogeneity of the blended fuel samples was ensured by running the blended samples through a ball mill before being stored.

2.2. Proximate and Ultimate Analysis of Fuel Blends

The ultimate analysis of the fuel samples was performed on a Thermo Fischer Scientific Flash Elementary analyser (EA 1112) using sample weights of approximately 1.8 mg. The Barnstead Thermolyne 6000 muffle furnace was used to perform the proximate analysis of the fuel based on the ISO 562:2010 and ISO 1171:2010 standards [37]. The oxygen and fixed carbon content were then determined using the difference method. To ensure results repeatability, each fuel sample was tested in triplicate.

2.3. Thermo-Gravimetric Analysis of Fuel Blends

Generally, thermo-gravimetric analysis investigates the degradation of substances under controlled heating environments. Variables such as the temperature range, heating rate, heating atmosphere, and sample particle size can be controlled during thermogravimetric analysis. As expected, these variables affect how the shape of the thermographs produced by the TGA [38]. When subjected to heat under an oxidative environment, solid fuels generally undergo drying, devolatilization, combustion, and ash formation steps either simultaneously or in parallel [39]. In as much as the degradation parameters obtained from the TGA are consistent against each other, practical pulverized fuel combustion setups operate with very high heating rates, which can reach 10,000 °C/s. This means the thermal parameters obtained from a TGA need to be modified slightly to produce comparable parameters for practical conditions [40].

The analysis was performed using a STA 7200 Hitachi thermal analyzer which was manipulated by the researchers as follows:

- Ceramic pan;
- 10 mg \pm 0.6 mg sample weights;
- 5, 12.5, and 20 °C/min heating rates;
- Nonisothermal temperature setting;
- 25–915 °C temperature range;
- 20 mL/min purge gas flow rate, (15.8 mL/min pure N₂ and 4.2 mL/min pure O₂), and
- 0.5 s data logging time.

The machine embedded workstation (TA 7000) managed to record the time (min), temperature (°C), differential thermal analysis (μ V), sample mass (μ g), and sample mass loss rate (μ g/min) on Microsoft excel format files. These data were then manipulated by the researchers using Origin Pro 2021 software to trace thermographs and evaluate the pertinent combustion parameters.

2.4. Theoretical Background

The Arrhenius equation was used to represent the reaction rate of the fuel sample degradation within the TGA over a specific time range as shown in Equation (1).

$$k(T) = A \cdot \exp\left(-\frac{E}{RT}\right) \quad (1)$$

where $k(T)$ represents the reaction rate constant, E the activation energy (kJ/mol), R the universal gas constant (8.314 J/mol.K), A the pre-exponential factor, and T the temperature (K). The degree or extent of degradation was represented by Equation (2).

$$\alpha = \frac{M_0 - M_t}{M_0 - M_f} \quad (2)$$

where M_0 represents the initial weight, M_t the sample weight at time t and M_f the final weight [41,42]. The sample mass loss rate curve (DTG) was acquired by first-order differentiation of the sample mass curve (TG). Since combustion occurs in stages, different zones of analysis had to be demarcated on the TGA/DTG curves permitting a modular approach of accurately determining the kinetic triplicate parameters of the rate equation (Activation energy, pre-exponential factor, and reaction rate constant). One easy approach that was used to make the reaction zones apparent was to superimpose the TG curve and DTG curve. Through visualizing the inflection points and high gradient sections that appear on the DTG curve, high reaction zones and points of maximum mass loss rate could be made apparent [38,43]. In summary, Figures 1 and 2 represent the TGA/DTG curve, and important points used to determine the pertinent combustion index parameters.

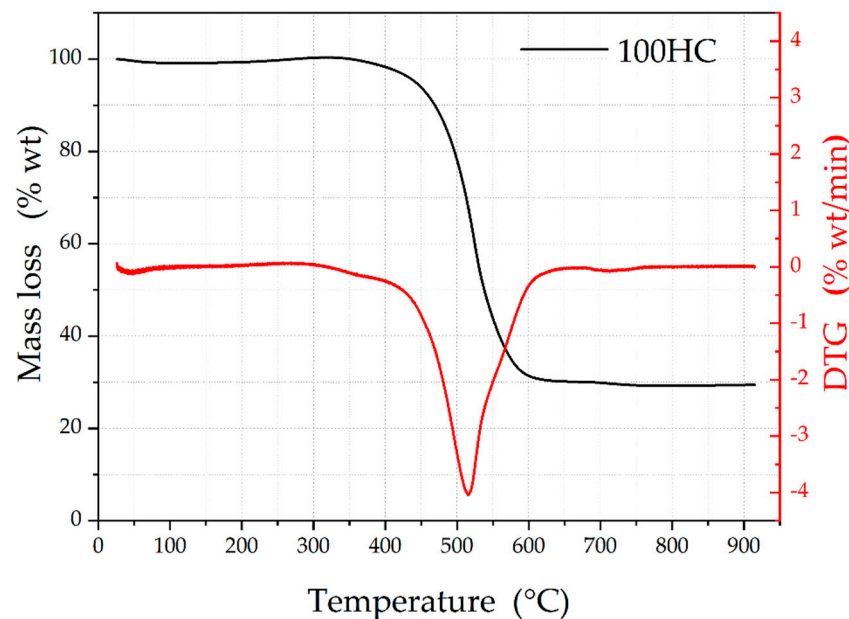


Figure 1. TG/DTG curves for 100HC at 5 °C/min heating rate under an air atmosphere.

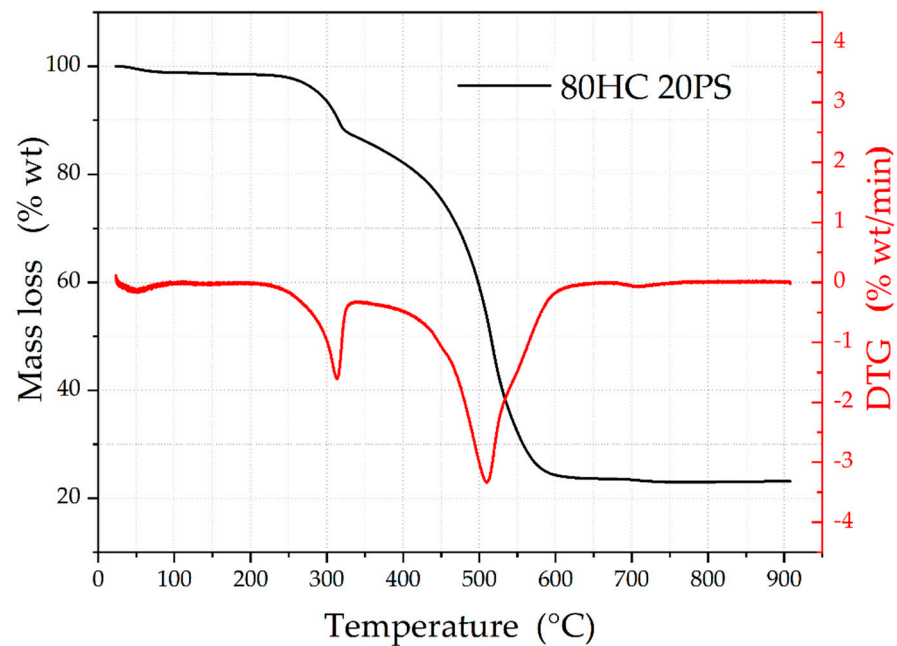


Figure 2. TG and DTG curves for 80HC 20PS at 5 °C/min heating rate under an air atmosphere.

Where T_{init} denotes the temperature at the beginning of the experiment. This corresponds to the starting of the first stage which corresponds to initial mass loss due through moisture loss. T_1 then represents the temperature at the end of stage 1 and beginning of the stage 2, which is around 115 °C for most experiments (saturation temperature of H_2O at 1 atm is 100 °C). Stage 2 marks the beginning of physical and chemical oxygen adsorption, which results in a slight increase of sample mass. During chemical adsorption, oxygen containing complexes are formed on the surface. This phenomenon is generally more pronounced for coal rather than biomass [44]. T_{ig} represents the temperature at the ignition point which then corresponds to the beginning of stage 3. Using the DTG curve, the ignition point is marked when the mass loss rate first becomes equivalent to 1% wt./min [17,39]. After the fuel ignites, another point of interest to researchers that is made apparent by superimposing the DTG curve is the point which corresponds to maximum mass loss rate or the point with the highest gradient on the TG curve. The point is derived from the minimum inflection point on the DTG curve (DTG_{max}) which then corresponds to a temperature T_{max} . DTG_{max} is represented by Equation (3).

$$DTG_{max} = \left| \left(\frac{d\alpha}{dt} \right)_{max} \right| \quad (3)$$

Bermejo et al. [45] highlighted that the weight loss peak is due to the formation of CO_2 and CO in large amounts. Stage 3 ends at burnout point which is derived from the DTG curve as well as corresponding to a mass loss rate of 1% wt./min after passing T_{max} [17,46]. The temperature at burnout is denoted by T_b and final experimental temperature is represented as T_{fin} .

Having derived the pertinent data from the TG/DTG curves, necessary combustion parameters are then calculated based on the data extracted. Of interest to this research were the:

- ignition index (Φ_{ig});
- burnout index (Φ_b);
- devolatilization index (Φ_d);
- 1st combustion index (Ψ_1) or combustion characteristic factor (CCF), and
- 2nd combustion index (Ψ_2).

The ignition index (Φ_{ig}) is used to highlight the ignition reactivity of the fuel samples. A larger ignition index is representative of combustion occurring easily at lower temperatures. The burnout index (Φ_b) is used to highlight the ability of a fuel sample to combust completely [21,47]. The ignition index and the burnout index are derived from the maximum mass loss rate (DTG_{max}) as represented by Equations (4) and (5), respectively [48]. Physically, a fuel sample can only be ignited once as highlighted in Figure 2 though the DTG curve for a blended sample makes apparent multiple peaks. As such, in support with the findings by Jiang et al. [17] and Urban et al. [39], the two DTG_{max} values obtained at the two local peaks can be averaged and used to evaluate the overall ignition index. This meant average(t_{max}) represents the average time for the two local peaks occurrence, whilst average($\Delta t_{1/2}$) represents the average of the time ranges when $|DTG| > |DTG_{max}|/2$.

$$\Phi_{ig} = \frac{\text{average}(DTG_{max})}{t_{ig} \cdot \text{average}(t_{max})} \quad (4)$$

$$\Phi_b = \frac{\text{average}(DTG_{max})}{\text{average}(\Delta t_{1/2}) \cdot \text{average}(t_{max}) \cdot t_b} \quad (5)$$

where t_{ig} represents the time at ignition and t_b the time at the final burnout.

The other indexes related to the temperature at the specific points are devolatilization index (Φ_d), 1st combustion index (Ψ_1), and 2nd combustion index (Ψ_2). The devolatilization index is more influential when the material has high-volatile content [45]. The 1st combustion index highlights the combustion activity that a fuel sample possesses [39,49]. The 2nd combustion index highlights the intensity and rate of the combustion process [50,51]. Equations (6)–(8) represent the formulas used to derive the devolatilization index, 1st combustion index, and 2nd combustion index.

$$D_i = \frac{\text{average}(DTG_{max})}{[\text{average}(T_{max}) - T_{ig}] \cdot \text{average}(T_{max})} \quad (6)$$

$$\Psi_1 = \frac{\text{average}(DTG_{max}) \cdot DTG_{mean}}{(T_{ig})^2 \cdot T_b} \quad (7)$$

$$\Psi_2 = \text{average}(T_{max}) \cdot \ln\left(\frac{\text{average}(\Delta T_{1/2})}{DTG_{mean}}\right) \quad (8)$$

where DTG_{mean} represents the mean combustion rate, T_{ig} the local ignition temperature, T_b the final burnout temperature, $\text{average}(T_{max})$ the average of the local temperatures at maximum mass loss rates, and $\text{average}(\Delta T_{1/2})$ the corresponding temperature ranges when $|DTG| > |DTG_{max}|/2$.

2.5. Synergistic Effects

Synergy within the scope of this study focused on the combined effect of fuels under consideration towards different thermal parameters. Amplified, summative, or subdued effects were expected to manifest towards the thermal parameters due to fuel blending. As such, a synergistic effect value was calculated to determine the combined effect of certain combustion parameters against an expected theoretical value as given by Equation (9). These parameters included the mass loss, rate of mass loss, and combustion indexes.

$$C = \frac{U_{\text{experimental}}}{\sum k_i U_i} - 1 \quad (9)$$

where C represents the synergistic effect coefficient ($C < 0$ negative synergy; $C = 0$ no synergy; $C > 0$ positive synergy), $U_{\text{experimental}}$ the experimental combustion parameter of the fuel blend, k_i the mass fraction of the individual fuel within the blend, U_i the experimental combustion parameter of the individual fuel within the blend. The same equation though in different forms was used by Wu et al. [20] when studying copyrolysis of

coal and cellulose, Wang et al. [30] when studying cocombustion of coal and polyurethane, and Florentino–Madiedo et al. [52] when studying copyrolysis of torrefied sawdust, coal, and paraffin. From a statistical point of view, it is very important to understand that synergy can be determined from an additive, multiplicative, or empirical based point of view [53]. This study chose to implement the additive approach which assumes parameters must behave in a linear manner when they are combined, thus the averaging done on the denominator in Equation (9).

3. Results and Discussion

3.1. Fuel Physical and Chemical Properties

Sieve analysis produced particles with a minimum diameter of 25 microns and maximum diameter of 250 microns with regards to coal samples. Pinus sawdust sieve analysis produced particles with a minimum diameter of 75 microns and a maximum diameter of 250 microns. To assure homogeneity of particle sizes, the $180 < d_p \leq 250$ diameter group was used for all the subsequent analysis. The physical and chemical properties of coal, pine sawdust, and their fuel blends are presented in Table 2.

Table 2. Chemical properties of coal, pine sawdust, and fuel blends.

	Proximate Analysis * (weight %)			Ultimate Analysis * (weight%)				
	** Fixed Carbon	Volatile Matter	Ash	C	H	** O	N	S
100HC	53.97	23.10	22.93	58.671	2.946	13.245	1.613	0.593
90HC 10PS	48.21	29.91	21.88	58.489	3.367	14.246	1.448	0.570
80HC 20PS	46.35	31.82	21.83	56.954	3.734	15.632	1.296	0.555
70HC 30PS	46.02	33.74	20.24	56.885	4.093	17.100	1.143	0.535
100PS	15.62	80.68	3.70	49.504	6.035	40.404	0.358	0

* On a dry basis; ** By difference.

Several authors correlated the high-volatile content and low ash in Pinus sawdust as compared to that of coal regardless of the rank. Part of the fuels investigated by Murredu et al. [21] contained Pinus wood chips and South African bituminous coal, and those researched by Zhou et al. [19] contained sub-bituminous coal and sawdust blends, with both agreeing with the researchers findings. The oxygen and hydrogen content increased with Pinus sawdust blending whilst carbon, nitrogen, and sulfur decreased. Generally, because of the increased volatile content (hence, oxygen and hydrogen) from Pinus sawdust, combustion reactivity was expected to improve since hydrogen is more reactive than carbon and fuel-oxygen always helps in the combustion process. However, combustion stability was expected to reduce since hydrogen and its radicals tend to combust violently as compared to that of carbon and its radicals [54].

3.2. Effect of Blending Ratio on TG-DTG Curves

The thermal degradation (TG/DTG) curves for 100HC, 90HC10PS, 80HC20PS, 70HC30PS, and 100PS fuel blends under an oxidative atmosphere at 5 °C/min heating rate are represented in Figures 3 and 4.

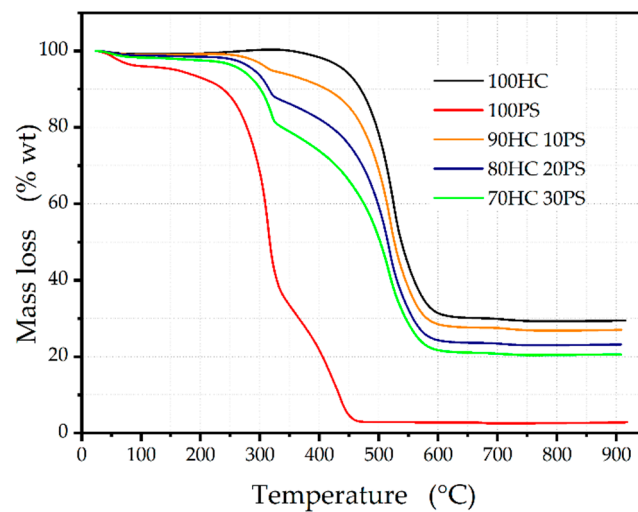


Figure 3. TG curves for all fuel samples at 5 °C/min heating rate under an air atmosphere.

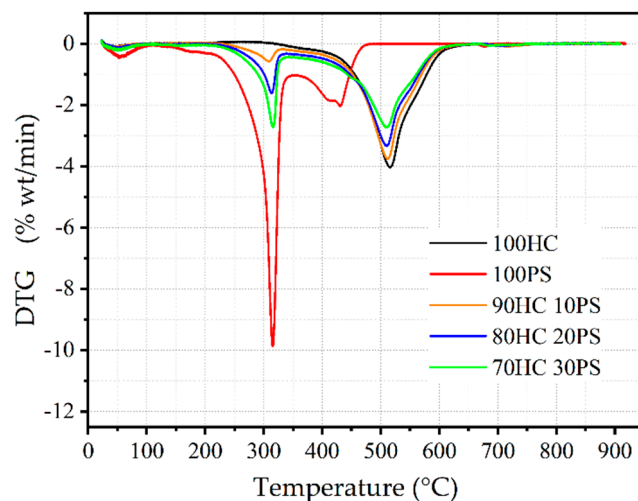


Figure 4. DTG for all fuel samples at 5 °C/min heating rate under an air atmosphere.

Figures 3 and 4 show an apparent initial mass gain for the 100HC fuel blend from the initial temperature to around 350 °C. Correlating with Figure 1, the first stage is highlighted as the initial mass loss phase due to inherent moisture loss. The first stage is demarcated by a temperature of around 115 °C for all blending ratios, as all moisture is expected to be liberated. The 100PS sample loses about 4% of its mass during stage 1, whilst the 100HC loses only 1% of its mass. This meant the biomass sample contained more inherent moisture than coal [55]. The second stage displays a distinct difference on the effect of physical and chemical adsorption of oxygen towards the fuel sample. As the biomass proportion increased, mass gain during stage 2 became less pronounced until mass loss was experienced during that stage. This effect was attributed to the coexistence of mass loss due to release of light volatiles (alkyl side chains and oxygen-containing functional groups) occurring at the same time as weight gain due to oxygen adsorption [44]. This resulted in fuel blends that contained more coal being able to adsorb oxygen more than they were able to release light volatiles. As such during stage 2, the 100HC sample experienced a quasimass gain of around 1%, whilst the 90HC10PS sample did not experience any mass change and the 100PS sample losing 8.4% of its initial weight. It is also important to note that as demonstrated on Figure 4, the DTG curves were generally close to the baseline during stage 1 and stage 2 due to the less pronounced mass loss.

Figures 3 and 4 show how synergistic effects of blending Pinus sawdust and coal are much more evident during Stage 3, which corresponds to the homogenous & heterogenous

combustion stage. Stage 3 commences at around the ignition temperature and ends at the burnout temperature. Rapid release of volatiles, homogenous volatile combustion, and heterogenous combustion of the remaining char are pronounced during this stage [43]. Adiabatic flame temperature is attained during this stage as well since heat release reaches its peak. Apart from the 100HC sample, a step is evident on the TG curve at around 315 °C for fuel samples that contain Pinus sawdust, which corresponds to the formation of another peak on the DTG curve at that temperature. According to the ultimate analysis of the coal and Pinus sawdust as presented in Table 2, Pinus sawdust contains a high volatile content than coal. As such, with volatiles having a lower flash point/ignition point than char, two peaks are formed on the DTG curve, with one signalling the prohomogenous volatile combustion zone followed by the other one which highlights a proheterogenous char combustion zone. Zhou et al. [19] highlighted why the first peak appears earlier than the second one, which is mainly due to volatile release when hemicellulose (220–315 °C), cellulose (315–400 °C), and part of lignin (137–667 °C) decompose when biomass is subjected to heat. The effect of high volatile content on the appearance of the DTG curve is also corroborated by Niu et al. [56] during their investigations with bituminous coal and municipal solid waste biomass. Figure 4 demonstrates how the prohomogenous volatile combustion DTG peak increased from 0.579 to 1.613, then 2.716 %wt./min for 90HC10PS, 80HC20PS, and 70HC30PS, respectively, signaling the increase in volatile composition. Homogenous volatile combustion is associated with higher reaction rates than heterogenous char combustion mainly because the former is based on volumetric combustion, whilst the latter is based on surface combustion [26].

The last stage corresponding to the burnout region generally occurred around the same temperature for the 5 °C/min heating rate. Termination of char combustion generally takes place during this stage [26]. By use of particle diameter group $180 \mu\text{m} < d_p \leq 250 \mu\text{m}$ for both coal and Pinus sawdust samples, any influence of particle size towards char combustion was removed. Char combustion is a surface process and char obtained from biomass has a higher porosity than char from coal. This tends to result in a higher surface area for biomass char which helps the overall burnout characteristics [31,57]. Consequently, the 100PS sample attains burnout at a lower temperature 445.90 °C as compared to samples that contain coal that tend to burnout at around 565 °C, corresponding to a 120 °C difference. The final weight percentage on the TG curve shows a decreasing trend as Pinus sawdust increased which is directly linked to the ash content in the fuel samples as shown in Table 2. By extension, the lesser the propensity to form ash towards the final stages of combustion, the more likely furnace fouling is reduced [19]. In summary, Figure 3 showed how the TG curves generally shifted from right to left highlighting increased mass loss at lower temperatures. Figure 4 showed how the DTG curves generally made apparent another peak as the blending ratio of Pinus sawdust was increased. The TG and DTG curves for 100HC display a general trend associated with most coal species of a smooth almost linear mass loss as well as a single peak on the DTG curve [58]. The TG and DTG curves for 100PS are mirrored by the findings of Bermejo et al. [45] as well during their investigations with quinoa plant residues. An interesting consistency for the DTG curves was the temperature at which maximum mass loss occurred. Looking at Figure 4, the left peak occurred at a temperature around 315.31 °C for all the samples which contained Pinus sawdust blends. Similarly, the right peak occurred at around 510 °C for all the samples which contained coal. This effect is attributed to the qualitative nature of volatiles and char for either Pinus sawdust or coal.

3.3. Synergistic Coefficients of TG-DTG Curves

Using Equation (9), the numerical value of synergy was determined for the mass loss and rate of mass loss for 90HC10PS, 80HC20PS, and 70HC30PS blends. Interaction between Pinus sawdust and coal was evident, thus the need to determine the level of synergy as a numerical value. Figure 5 shows the synergistic effect coefficient against temperature for the mass loss (TG) curves for the blends at 12.5 °C/min heating rate. The 80HC20PS and

70HC30PS blends showed weak positive synergy around 348 °C which matched the region where the step in Figure 3 appeared. This region is where the pro-homogenous volatile combustion took place. However, negative synergy was experienced after about 492 °C for all the fuel blends, which corresponds to the proheterogenous char combustion region. The expected mass loss due to Pinus sawdust blending was not experienced during this region, thus the negative synergy. Florentino–Madiedo et al. [52] obtained almost similar results with regards to coal biomass blending such that their synergy curves of mass loss were largely negative throughout the combustion process. Wu et al. [20] suggested that volatile generation generally results in a slightly positive synergistic coefficient towards mass loss as well.

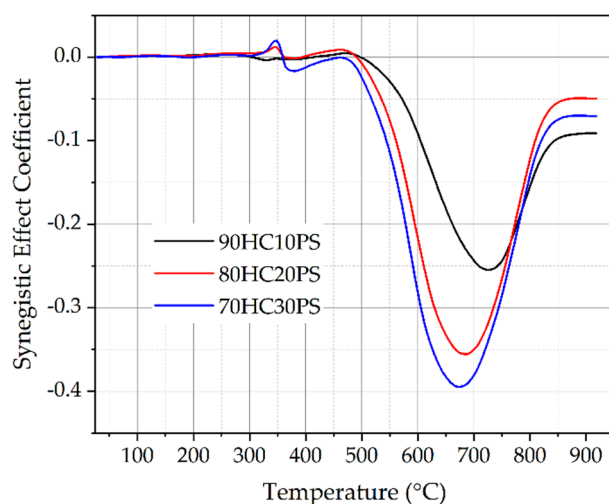


Figure 5. Degree of synergy towards TG curves for 90HC10PS, 80HC20PS, and 70HC30PS fuel samples at 12.5 °C/min heating rate under an air atmosphere.

Figure 6 shows the rate of mass loss synergy due to the blending of Pinus sawdust. The 80HC20PS and 70HC30PS blends experienced positive synergy until around 630 °C, which corresponds to the burnout point. This meant that the rate of mass loss for the 80HC20PS and 70HC30PS blended samples was increased greatly by Pinus sawdust throughout the combustion process unlike the 90HC10PS blend. As far as 80HC20PS and 70HC30PS blends are concerned, Figure 6 also shows blending increased the first peak to 5.5 and 8.8, respectively, which corresponded to initial volatile release, whilst the second peak increased to 2.6 and 6.8, respectively, which corresponded to the prohomogenous volatile combustion region. Wu et al. [20] noted how a large number of hydrogen containing free radicals and volatile intermediate products are formed more from biomass than coal. As such, rate of volatile release (first peak) and rate of volatile combustion (second peak) experienced the most influence. In summary, a blending ratio of 20% or higher showed better synergy towards rate of mass loss. This suggests that with regards to Pinus sawdust and coal, blending should be higher than 20% if the benefits towards combustion are to be experienced.

3.4. Effect of the Heating Rate on TG-DTG Curves

Comparison of heating rate under an oxidative environment was also investigated in this research. Figures 7 and 8 highlights the TG/DTG curves that were obtained for 5, 12.5, and 20 °C heating rates for the 90HC10PS sample. The concept of thermal lagging is made apparent by the difference in TG/DTG curves at different heating rates as shown in Figures 7 and 8. Thermal lagging is a phenomenon related to the zeroth law of thermodynamics, which is centered around thermal equilibrium between the sample and surroundings [59].

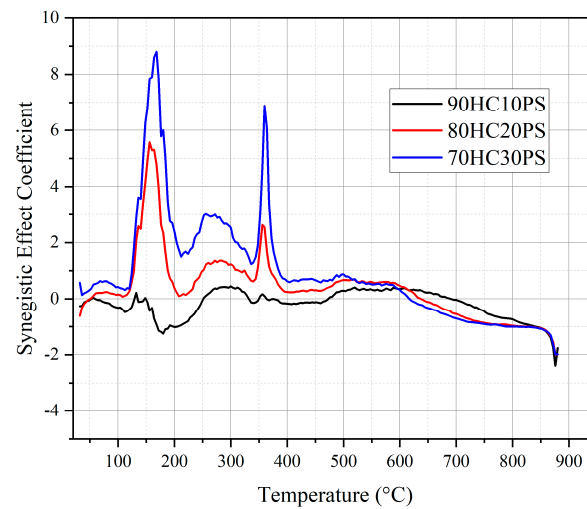


Figure 6. Degree of synergy towards DTG curves for 90HC10PS, 80HC20PS, and 70HC30PS fuel samples at 12.5 °C/min heating rate under an air atmosphere.

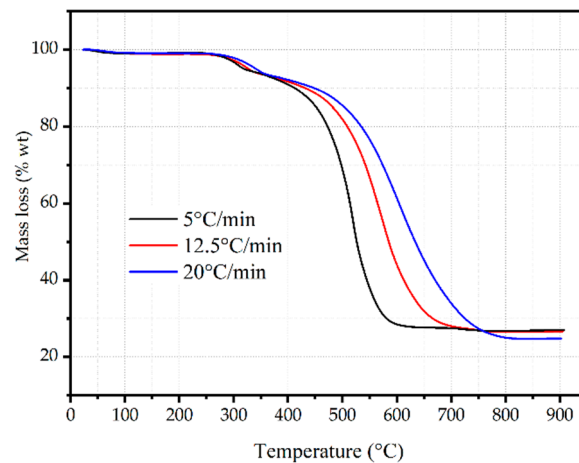


Figure 7. TG curves for 90HC10PS at 5, 12.5, and 20 °C/min heating rates under an air atmosphere.

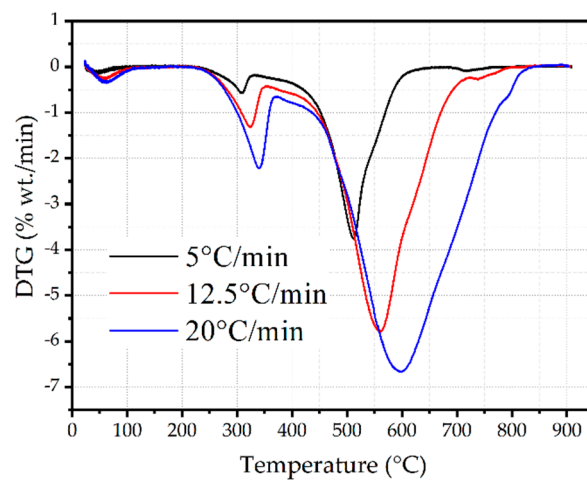


Figure 8. DTG curves for 90HC10PS at 5, 12.5, and 20 °C/min heating rates under an air atmosphere.

At high heating rates, the sample required more time to adjust to the effect of temperature, whilst at low heating rates the residence time was quite sufficient. As experienced by Chen et al. [58], an increase in heating rate pushes the high gradient zone on the TG curve to the right. Consequently, the rate of mass loss is also increased for higher heating

rates. Generally, regardless of the fuel blend composition, thermal lag resulted in a more spread-out TG curve when the heating rate was increased. Figure 8 shows the DTG curves for the 90HC10PS sample at different heating rates, the first peak corresponding to volatile interaction increased by 287%, whilst the second peak corresponding to the char interaction increased by 78.3% as heating rate was ramped up from 5 to 20 °C/min. The ignition temperature decreased by 33.7% from 452.11 °C to 299.81 °C, whilst the burnout temperature increased by 35.2% from 568.30 °C to 768.58 °C when heating rate was ramped up from 5 to 20 °C/min. Combustion within industrial boilers or drop tube furnaces occurs at very high heating rates of around 1000 °C/min, which by deduction tends to result in a lot of thermal lag. As such to assure complete combustion, a higher residence time is generally recommended when the sample attains the high temperatures [60]. Huang et al. [61] during their studies with coal on the effect of residence time towards release of volatiles supported the notion that fuel particles with a diameter of less than 64 microns are less likely to suffer the effect of decreased residence time; hence, increased heating rates. This meant that the best way to counter the thermal lag effects caused by high heating rates is to make sure the particle diameter is small enough.

3.5. Ignition, Devolatilization, Burnout, and Combustion Indexes

Based on Equations (4)–(7), combustion parameters were determined and evaluated for synergy. Table 3 summarizes the important points from the TG and DTG curves necessary to evaluate the combustion performance indexes.

Table 3. Important points on TG and DTG curves for various fuel blends in air atmosphere.

Heating Rate @ $\beta = 5$ °C/min							
	T_{ig} (°C)	t_{ig} (min)	T_{max} (°C)	t_{max} (min)	DTG_{max} %wt/min	T_b (°C)	t_b (min)
100HC	455.27	85.158	515.21	95.44	4.037	577.07	109.542
90HC 10PS	452.11	85.100	511.34	95.36	3.759	568.30	108.625
* 80HC 20PS	301.01	55.167	(312.62) 509.51	(57.18) 95.20	(1.608) 3.336	563.51	107.675
* 70HC 30PS	289.97	53.142	(315.92) 510.26	(57.37) 95.67	(2.716) 2.736	559.25	106.775
100PS	249.51	45.542	315.31	57.02	9.872	445.90	83.2
Heating Rate @ $\beta = 12.5$ °C/min							
	T_{ig}	t_{ig}	T_{max}	t_{max}	DTG_{max}	T_b	t_b
100HC	462.63	35.575	577.84	44.09	5.238	708.17	55.142
* 90HC 10PS	307.452	23.433	(323.773) 559.12	(24.625) 42.242	(1.323) 5.790	670.44	52.092
* 80HC 20PS	280.6285	21.475	(323.70) 548.43	(24.625) 41.658	(2.391) 6.001	655.34	51.092
* 70HC 30PS	266.366	20.408	(327.07) 540.36	(24.75) 41.108	(5.447) 5.366	634.50	49.417
Heating Rate @ $\beta = 20$ °C/min							
	T_{ig}	t_{ig}	T_{max}	t_{max}	DTG_{max}	T_b	t_b
100HC	457.70	22.267	605.66	29.12	5.741	820.05	39.725
* 90HC 10PS	299.81	14.892	(340.19) 599.30	(16.63) 28.86	(2.221) 6.673	768.58	37.625
80HC 20PS	281.38	14.008	573.17	27.125	7.271	717.25	35.133
70HC 30PS	265.76	13.342	350.68	16.458	10.748	699.96	34.300
100PS	197.91	10.333	341.82	16.32	34.403	498.81	24.158

* DTG = 1% wt./min at four separate points.

The ignition temperature of the fuel blends containing Pinus sawdust were significantly lower when compared to that of 100HC mainly due to the presence of volatiles released from Pinus sawdust, as supported by Kongkaew et al. [50] during their investigations with blends containing rice straw. Pinus sawdust generally improved the ignition temperature, which is demonstrated by the decrease from around 450 °C to less than 300 °C for the 5 °C/min heating rate. However, at a heating rate of 5 °C/min, it was apparent that the ignition temperature did not improve significantly between the 100HC and 90HC10PS fuel samples. Thus, to offset benefits of blending on ignition, the researchers proposed fuel substitution by mass above 10%. Figure 9 then summarizes the comparisons between the ignition temperature of the fuel samples at different heating rates. The error bars were too small to be visible on Figure 10 because the simultaneous TGA instrument had hypersensitivity of $\pm 0.1 \mu\text{g}$. This translated to very small uncertainties for the repeated experiments, e.g., the 100HC sample at a heating rate of 5 °C/min had an uncertainty of 0.001772 °C towards its ignition temperature.

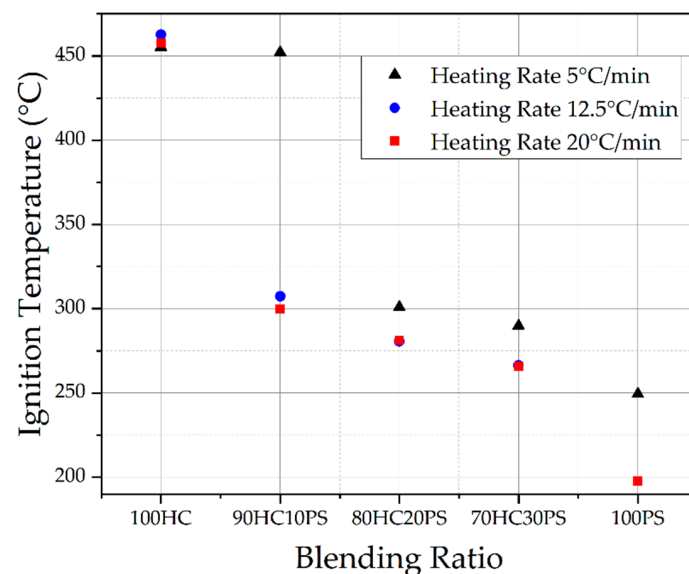


Figure 9. Ignition temperature variation for fuel blends at 5 °C/min and 20 °C/min heating rate under an air atmosphere.

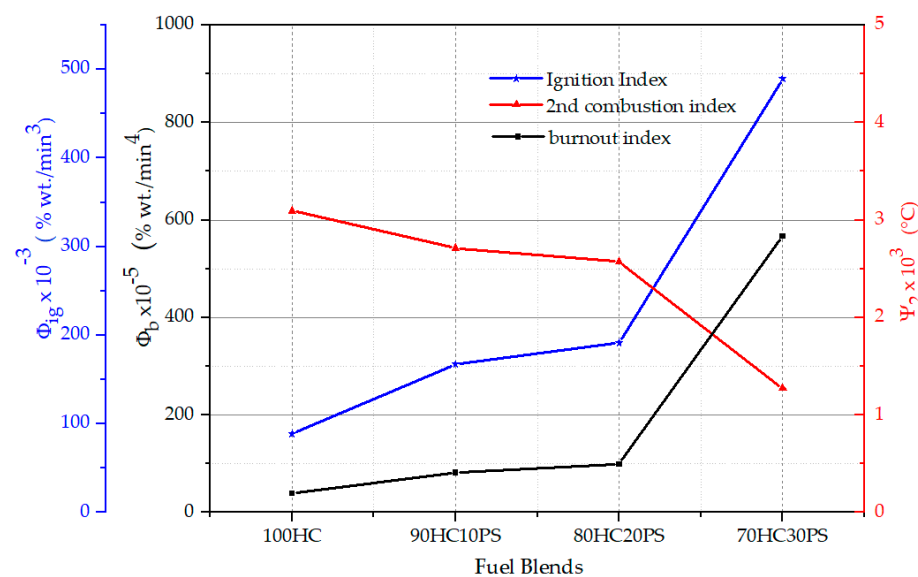


Figure 10. Ignition index, burnout index, and second combustion index at 20 °C/min heating rate under an air atmosphere.

As highlighted in Table 3, the slower heating rate of 5 °C/min showed a decreasing trend in maximum mass loss rate as blending increased, whilst the effect was reversed for the higher heating rate of 20 °C/min. Riaza et al. [24] suggested that this phenomenon can be explained by the existence of a volatile cloud around the fuel particle, which, in turn, hinders diffusion of oxygen to and from the surface of the fuel. As such, two contracting effects exist at the same time which are char reaction vs. volatile cloud formation [62]. Because temperature has a direct relationship on diffusivity, higher heating rates tend to promote diffusion of oxygen towards the particle surface [26]. At higher heating rates, the effect of volatile cloud formation vs. char reaction seemed to sway in the favor of char reaction mainly because the effect of temperature on diffusivity.

From a qualitative point of view, when considering a certain heating rate, the DTG peak for prohomogenous volatile combustion occurred around the same time regardless of the fuel blending ratio (e.g., ≈ 315 °C and 57 min for a 5 °C/min heating rate). The same phenomenon existed for the DTG peak corresponding to proheterogenous combustion (e.g., ≈ 510 °C and 95 min for a 5 °C/min heating rate). This aspect of DTG peak analysis is useful since each individual constituent has a respective temperature and time at which a DTG peak occurs. This meant that as long as the blend contained Pinus sawdust, a DTG peak was expected around 315 °C at 57 min if the heating rate is 5 °C/min with the same reasoning applicable for other heating rates. Though not explained in detail, Zhou et al. [19], Jiang et al. [17], Li et al. [22], and Yan et al. [49] produced similar trends for blended coal and biomass samples.

Table 4 then gives the overview of all the combustion parameters calculated using Equations (4)–(8) and data from Table 3. Figure 10 demonstrates the trends observed for the ignition index, burnout index, and second combustion index at 20 °C/min heating rate under an air atmosphere. As shown in Figure 10, the ignition index of the fuel blends increased with increasing blending ratio of Pinus sawdust. As highlighted by other authors, the higher the ignition index, the higher the propensity for combustion at lower temperatures or occurrence of significant combustion at lower temperatures [47,50]. The effect is mirrored by the first combustion index (Ψ_1), which is related to combustion activity. As the blending increased, the actual combustion activity increased supported by the volatiles released from biomass. According to Equation (7), the first combustion index is directly proportional to DTG_{mean} , which generally increased with blending and inversely proportional to burnout temperature which generally decreased with blending. As such, the general trend for first combustion index was an increase as blending increased. Niu et al. [56] supported the view and further highlighted the relationship between heating rate, ignition index, and first combustion index. Their results showed better ignition and burnout indexes are directly proportional to heating rate which was corroborated by the authors findings.

The burnout index increased with blending ratio of Pinus sawdust. Burnout is closely related to char combustion, and based on Equation (6), the index is inversely proportional to burnout time. Char from biomass is acknowledged to be more porous than that from coal, which then aids the surface combustion activity of biomass, thus increasing the burnout index. As demonstrated in Table 3, burnout time decreased with blending thus the calculated burnout index increased. As demonstrated by Zhou et al. [19] with their cocombustion experiments of coal and sawdust, burnout index showed a similar trend with the findings of this study. The second combustion index which is related to the intensity and stability of combustion showed a decreasing trend with blending ratio. Equation (8) demonstrates the second combustion index is heavily dependent on $\Delta T_{1/2}$, a parameter related to stability, and DTG_{mean} a parameter related to intensity. By deduction, stability of combustion was decreased by biomass blending. Comparison of stability index amongst heating rates showed that at a heating rate of 5 °C/min, the 2nd combustion index decreased by 1% as blending increased to 30%, whilst the index decreased by 60.8% and 58.8% at 12.5 °C/min and 20 °C/min, respectively. This meant that in as much as the other combustion parameters were increased by blending, a balance is necessary since

combustion stability is decreased in turn [63]. In summary, blending did not result in a linear variation of combustion indexes. Optimization is thus needed in such a way that the gains and losses are balanced with regards to combustion indexes.

Table 4. Derived combustion parameters from TG and DTG curves for various fuel blends in air atmosphere.

Heating Rate @ $\beta = 5 \text{ }^\circ\text{C/min}$								
	DTG_{mean} %wt min	$\Delta T_{1/2}$ ($^\circ\text{C}$)	$\Delta t_{1/2}$ (min)	$\Phi_{ig} \times 10^{-4}$ %wt min ³	$\Phi_b \times 10^{-5}$ %wt min ⁴	$D_i \times 10^{-4}$ %wt ² min. $^\circ\text{C}^2$	$\Psi_1 \times 10^{-8}$ %wt ² min ² . $^\circ\text{C}^3$	$\Psi_2 \times 10^3$ $^\circ\text{C}$
100HC	0.4033	68.57	13.93	4.9670	2.7730	1.3072	1.3612	2.6461
90HC 10PS	0.4171	68.54	13.88	4.6321	2.6154	1.2411	1.3499	2.6087
80HC 20PS	0.4390	69.70	14.22	6.3520	2.2892	0.3140	2.8685	2.5819
70HC 30PS	0.4538	77.75	15.84	5.3815	1.6907	0.2434	2.6403	2.6246
Heating Rate @ $\beta = 12.5 \text{ }^\circ\text{C/min}$								
	DTG_{mean}	$\Delta T_{1/2}$	$\Delta t_{1/2}$	$\Phi_{ig} \times 10^{-4}$	$\Phi_b \times 10^{-5}$	$D_i \times 10^{-4}$	$\Psi_1 \times 10^{-8}$	$\Psi_2 \times 10^3$
100HC	1.01259	156.84	12.542	33.395	17.179	0.7868	34994	2.9139
90HC 10PS	1.0385	123.64	9.992	58.493	26.335	0.4115	9.4883	2.6724
80HC 20PS	1.1079	110.49	8.992	67.080	31.357	0.4086	12.8820	2.5241
70HC 30PS	1.1615	38.06	2.675	102.480	166.490	2.7435	14.0530	1.1413
Heating Rate @ $\beta = 20 \text{ }^\circ\text{C/min}$								
	DTG_{mean}	$\Delta T_{1/2}$	$\Delta t_{1/2}$	$\Phi_{ig} \times 10^{-4}$	$\Phi_b \times 10^{-5}$	$D_i \times 10^{-4}$	$\Psi_1 \times 10^{-8}$	$\Psi_2 \times 10^3$
100HC	1.5717	260.70	12.58	89.00	39.44	0.6406	5.2525	3.0957
90HC 10PS	1.6892	192.97	9.57	167.25	82.12	0.4152	17.0470	2.7135
80HC 20PS	1.7222	152.93	7.70	191.36	99.09	0.4348	22.0510	2.5714
70HC 30PS	1.7913	67.73	3.36	489.47	566.90	3.6092	38.9440	1.2739

4. Conclusions

Blending of Hwange bituminous coal and Pinus sawdust was investigated within this paper at different mass blending ratios with the aim of determining important combustion indexes. To the knowledge of the researchers, no similar studies were reported on the ignition, burnout, or 2nd combustion index of blended Hwange bituminous coal and Pinus sawdust.

- During the index determination by use of TG/DTG curves, synergistic effects were observed between the coal and Pinus sawdust blends. The mass loss curves (TG) for the 90HC10PS, 80HC20PS, and 70HC30PS blends demonstrated zero synergy from the initial temperature to around 492 $^\circ\text{C}$. Negative synergistic effects were observed between 492 $^\circ\text{C}$ and the final temperature. The rate of mass loss curves (DTG) demonstrated positive synergy from the initial temperature until around 600 $^\circ\text{C}$, then negative synergy until the final temperature for the 80HC20PS and 70HC30PS blends only.
- Ignition temperature was generally reduced from an average 460 $^\circ\text{C}$ to around 260 $^\circ\text{C}$ regardless of the heating rate. The ignition index thus increased with PS blending ratio though no linear relation was deduced. Burnout temperature was reduced by an average 14.6% between 100HC and 70HC30PS blending at 20 $^\circ\text{C}/\text{min}$ heating rate. Similarly, the burnout index increased as Pinus sawdust increased.
- The 2nd combustion index reflective of stability reduced as Pinus sawdust increased with a gradual decrease of 16.9% between 100HC and 80HC20PS, and a steeper decrease of 50.5% between 80HC20PS and 70HC30PS.
- Evaluation of TG/DTG curves and combustion indexes suggested an optimum blending ratio of 20% Pinus sawdust so that the benefits of cocombusting Hwange coal and Pinus sawdust are derived. Each fuel blend has optimum blending ratios as reported by other researchers, thus the need to specifically know the optimum cocombustion parameters with regards to Hwange coal and Pinus sawdust.

Blending of Hwange coal and pinus sawdust is recommended since important thermal combustion parameters are improved. This research in turn guides policy in terms of uptake of cocombustion technologies of Hwange coal and Pinus sawdust.

Author Contributions: Conceptualization, G.T.M.; formal analysis, G.T.M.; funding acquisition, D.M.M.; investigation, G.T.M.; methodology, G.T.M. and C.H.C.; resources, D.M.M. and P.G.N.; supervision, D.M.M.; visualization, G.T.M.; writing—original draft, G.T.M.; writing—review & editing, G.T.M., D.M.M., P.G.N. and C.H.C. All authors have read and agreed to the published version of the manuscript.

Funding: This research received no external funding.

Data Availability Statement: The data presented in this study is available on request from the corresponding author. The data is not publicly available because it's part of a PhD thesis.

Acknowledgments: Special thanks to both University of Johannesburg, South Africa and Chinhoyi University of Technology, Zimbabwe for supporting the author during his research.

Conflicts of Interest: The authors declare no conflict of interest.

References

1. Jingura, R.M.; Musadamba, D.; Kamusoko, R. A review of the state of biomass energy technologies in Zimbabwe. *Renew. Sustain. Energy Rev.* **2013**, *26*, 652–659. [CrossRef]
2. World Bank. Group Energy Use (kg of Oil Equivalent per Capita)—Zimbabwe. Available online: <https://data.worldbank.org/ujlink.uj.ac.za/indicator/EG.USE.PCAP.KG.OE?locations=ZW> (accessed on 1 September 2021).
3. Charis, G.; Danha, G.; Muzenda, E. A Review of the application of GIS in biomass and solid waste supply chain optimization: Gaps and opportunities for developing nations. *Detritus* **2019**, *6*, 1–11. [CrossRef]
4. Hyde, M.; Wursten, B.; Ballings, P.; Palgrave Coates, M. Flora of Zimbabwe: Species Information: *Pinus patula*. Available online: https://www.zimbabweflora.co.zw/speciesdata/species.php?species_id=102970 (accessed on 26 May 2021).
5. Mtshali, L.; Dlamini, M.; Kohler, N. The Opportunities and Challenges of Wood Waste Biomass and a Case Study on Biofuels in South Africa. In Proceedings of the Institute of Waste Management of Southern Africa, Johannesburg, South Africa, 30 September–4 October 2018; pp. 350–355.
6. Hancox, P.J. The Coalfields of South-Central Africa: A Current Perspective. *Episodes* **2016**, *39*, 407–428. [CrossRef]
7. Makomo Resources Coal Products. Available online: <https://makomoresources.com/coal-products/> (accessed on 2 September 2021).
8. Ma, W.; Zhou, H.; Zhang, J.; Zhang, K.; Liu, D.; Zhou, C.; Cen, K. Behavior of Slagging Deposits during Coal and Biomass Co-combustion in a 300 kW Down-Fired Furnace. *Energy Fuels* **2018**, *32*, 4399–4409. [CrossRef]
9. Mandø, M.; Rosendahl, L.A.; Yin, C.; Sørensen, H. Pulverized straw combustion in a low-NO_x multifuel burner: Modeling the transition from coal to straw. *Fuel* **2010**, *89*, 3051–3062. [CrossRef]
10. Tillman, D.A. Biomass cofiring: The technology, the experience, the combustion consequences. *Biomass Bioenergy* **2000**, *19*, 365–384. [CrossRef]
11. Cong, K.; Han, F.; Zhang, Y.; Li, Q. The investigation of co-combustion characteristics of tobacco stalk and low rank coal using a macro-TGA. *Fuel* **2019**, *237*, 126–132. [CrossRef]
12. Savolainen, K. Co-firing of biomass in coal-fired utility boilers. *Appl. Energy* **2003**, *74*, 369–381. [CrossRef]
13. Liu, Q.; Zhong, W.; Tang, R.; Yu, H.; Gu, J.; Zhou, G.; Yu, A. Experimental tests on co-firing coal and biomass waste fuels in a fluidised bed under oxy-fuel combustion. *Fuel* **2021**, *286*, 119312. [CrossRef]
14. Magida, N.E.; Bolo, L.L.; Hlangothi, S.P.; Dugmore, G.; Ogunlaja, A.S. Co-combustion Characteristics of coal-Scenedesmus Microalgae Blends and Their Resulting Ash. *Combust. Sci. Technol.* **2021**, *193*, 419–436. [CrossRef]
15. Chen, C.; Chan, Q.N.; Medwell, P.R.; Heng Yeoh, G. Co-Combustion Characteristics and Kinetics of Microalgae *Chlorella Vulgaris* and Coal through TGA. *Combust. Sci. Technol.* **2020**, *192*, 26–45. [CrossRef]
16. Chen, X.; Liu, L.; Zhang, L.; Zhao, Y.; Zhang, Z.; Xie, X.; Qiu, P.; Chen, G.; Pei, J. Thermogravimetric analysis and kinetics of the co-pyrolysis of coal blends with corn stalks. *Thermochim. Acta* **2018**, *659*, 59–65. [CrossRef]
17. Jiang, X.; Wang, C.; Wang, X.; Liu, Y.; Song, Z.; Lin, Q. Co-combustion of coal and carbonaceous wastes: Thermogravimetric analysis. *Energy Sources Part A Recovery Util. Environ. Eff.* **2019**, 1–15. [CrossRef]
18. Wang, C.; Wu, Y.; Liu, Q.; Yang, H. Study of the characteristics of the ashing process of straw/coal combustion. *Fuel* **2011**, *90*, 2939–2944. [CrossRef]
19. Zhou, C.; Liu, G.; Wang, X.; Qi, C. Co-combustion of bituminous coal and biomass fuel blends: Thermochemical characterization, potential utilization and environmental advantage. *Bioresour. Technol.* **2016**, *218*, 418–427. [CrossRef] [PubMed]
20. Wu, Z.; Zhang, J.; Zhang, B.; Guo, W.; Yang, G.; Yang, B. Synergistic effects from co-pyrolysis of lignocellulosic biomass main component with low-rank coal: Online and offline analysis on products distribution and kinetic characteristics. *Appl. Energy* **2020**, *276*, 115461. [CrossRef]

21. Mureddu, M.; Dessì, F.; Orsini, A.; Ferrara, F.; Pettinau, A. Air-and oxygen-blown characterization of coal and biomass by thermogravimetric analysis. *Fuel* **2018**, *212*, 626–637. [[CrossRef](#)]
22. Li, H.; Li, Y.; Jin, Y. Co-combustion Analyses of Coal and Sewage Sludge with High Moisture Content. *Energy Sources Part. A Recover. Util. Environ. Eff.* **2015**, *37*, 1896–1903. [[CrossRef](#)]
23. Boumanchar, I.; Chhiti, Y.; M'hamdi Alaoui, F.E.; Elkhrouakhi, M.; Sahibed-dine, A.; Bentiss, F.; Jama, C.; Bensitel, M. Investigation of (co)-combustion kinetics of biomass, coal and municipal solid wastes. *Waste Manag.* **2019**, *97*, 10–18. [[CrossRef](#)]
24. Riaza, J.; Álvarez, L.; Gil, M.V.; Pevida, C.; Pis, J.J.; Rubiera, F. Effect of oxy-fuel combustion with steam addition on coal ignition and burnout in an entrained flow reactor. *Energy* **2011**, *36*, 5314–5319. [[CrossRef](#)]
25. Akhtar, J.; Yaseen, A.; Munir, S. Effect of rice husk co-combustion with coal on gaseous emissions and combustion efficiency. *Energy Sources Part. A Recover. Util. Environ. Eff.* **2018**, *40*, 1010–1018. [[CrossRef](#)]
26. Turns, S. *An Introduction to Combustion: Concepts and Applications*, 2nd ed.; McGraw-Hill Series in Mechanical Engineering; McGraw-Hill: New York, NY, USA, 1996; ISBN 9780077418946.
27. Gao, H.; Runstedtler, A.; Majeski, A.; Boisvert, P.; Campbell, D. Optimizing a woodchip and coal co-firing retrofit for a power utility boiler using CFD. *Biomass Bioenergy* **2016**, *88*, 35–42. [[CrossRef](#)]
28. Xing, X.; Wang, S.; Zhang, Q. Thermogravimetric Analysis and Kinetics of Mixed Combustion of Waste Plastics and Semicoke. *J. Chem.* **2019**, *2019*, 10. [[CrossRef](#)]
29. Haykiri-Acma, H.; Yaman, S. Synergistic investigation for co-combustion of biochars and lignite-thermogravimetric analysis approach. *J. Therm. Sci. Eng. Appl.* **2019**, *11*, 011006. [[CrossRef](#)]
30. Wang, H.; Tian, Y.; Chen, X.; Li, J. Kinetic and Synergetic Effect Analysis of the Co-Combustion of Coal Blended with Polyurethane Materials. *ACS Omega* **2020**, *5*, 26005–26014. [[CrossRef](#)]
31. Chen, G.B.; Chatelier, S.; Lin, H.T.; Wu, F.H.; Lin, T.H. A study of sewage sludge co-combustion with Australian black coal and shiitake substrate. *Energies* **2018**, *11*, 3436. [[CrossRef](#)]
32. Tang, R.; Liu, Q.; Zhong, W.; Lian, G.; Yu, H. Experimental Study of SO₂ Emission and Sulfur Conversion Characteristics of Pressurized Oxy-Fuel Co-combustion of Coal and Biomass. *Energy Fuels* **2020**, *34*, 16693–16704. [[CrossRef](#)]
33. Zhou, C.; Gao, F.; Yu, Y.; Zhang, W.; Liu, G. Effects of Gaseous Agents on Trace Element Emission Behavior during Co-combustion of Coal with Biomass. *Energy Fuels* **2020**, *34*, 3843–3849. [[CrossRef](#)]
34. Ndou, N.R.; Bada, S.O.; Falcon, R.S.M.S.; Weiersbye, I.M. Co-combustion of *Searsia lancea* and *Tamarix usneoides* with high ash coal. *Fuel* **2020**, *267*, 117282. [[CrossRef](#)]
35. Ministry of Energy and Power Development. *National Renewable Energy Policy*; Ministry of Energy and Power Development: Harare, Zimbabwe, 2019.
36. Department of Minerals and Energy. *Renewable Energy Policy*; Department of Minerals and Energy: Pretoria, South Africa, 2004.
37. Zhu, Q. *Coal Sampling and Analysis Standards*; IEA Clean Coal Centre: London, UK, 2014.
38. Seifali Abbas-Abadi, M.; Fathi, M.; Ghadiri, M. Effect of Different Process Parameters on the Pyrolysis of Iranian Oak Using a Fixed Bed Reactor and TGA Instrument. *Energy Fuels* **2019**, *33*, 11226–11234. [[CrossRef](#)]
39. Urban, B.; Shirazi, Y.; Maddi, B.; Viamajala, S.; Varanasi, S. Flash Pyrolysis of Oleaginous Biomass in a Fluidized-Bed Reactor. *Energy Fuels* **2017**, *31*, 8326–8334. [[CrossRef](#)]
40. Authier, O.; Thunin, E.; Plion, P.; Porcheron, L. Global Kinetic Modeling of Coal Devolatilization in a Thermogravimetric Balance and Drop-Tube Furnace. *Energy Fuels* **2015**, *29*, 1461–1468. [[CrossRef](#)]
41. Niu, S.L.; Lu, C.M.; Han, K.H.; Zhao, J.L. Thermogravimetric analysis of combustion characteristics and kinetic parameters of pulverized coals in oxy-fuel atmosphere. *J. Therm. Anal. Calorim.* **2009**, *98*, 267–274. [[CrossRef](#)]
42. Li, H.; Niu, S.; Lu, C.; Wang, Y. Comprehensive Investigation of the Thermal Degradation Characteristics of Biodiesel and Its Feedstock Oil through TGA–FTIR. *Energy Fuels* **2015**, *29*, 5145–5153. [[CrossRef](#)]
43. Lü, H.F.; Deng, J.; Li, D.J.; Xu, F.; Xiao, Y.; Shu, C.M. Effect of oxidation temperature and oxygen concentration on macro characteristics of pre-oxidised coal spontaneous combustion process. *Energy* **2021**, *227*, 120431. [[CrossRef](#)]
44. Wang, H.; Tian, Y.; Li, J.; Chen, X. Experimental study on thermal effect and gas release laws of coal-polyurethane cooperative spontaneous combustion. *Sci. Rep.* **2021**, *11*, 1994. [[CrossRef](#)]
45. Bermejo, S.P.; Prado-guerra, A.; Isabel, A.; García, P.; Fernando, L.; Prieto, C.; Paniagua Bermejo, S.; Prado-guerra, A.; García Pérez, A.I.; Calvo Prieto, L.F. Study of quinoa plant residues as a way to produce energy through thermogravimetric analysis and indexes estimation. *Renew. Energy* **2020**, *146*, 2224–2233. [[CrossRef](#)]
46. Wang, C.; Zhang, Y.; Wang, P.; Zhang, J.; Du, Y.; Che, D. Effects of silicoaluminate oxide and coal blending on combustion behaviors and kinetics of zhundong coal under oxy-fuel condition. *J. Therm. Anal. Calorim.* **2018**, *134*, 1975–1986. [[CrossRef](#)]
47. Xu, T.; Ning, X.; Wang, G.; Liang, W.; Zhang, J.; Li, Y.; Wang, H.; Jiang, C. Combustion characteristics and kinetic analysis of co-combustion between bag dust and pulverized coal. *Int. J. Miner. Metall. Mater.* **2018**, *25*, 1412–1422. [[CrossRef](#)]
48. Korotkikh, A.G.; Slyusarskiy, K.V.; Larionov, K.B.; Osipov, V.I. Comparison of coal reactivity during conversion into different oxidizing medium. *J. Phys. Conf. Ser.* **2016**, *754*, 052005. [[CrossRef](#)]
49. Yan, Y.F.; Zhang, Z.E.; Zhang, L.; Zhang, L. Influence of coal properties on the co-combustion characteristics of low-grade coal and city mud. *Glob. NEST J.* **2014**, *16*, 329–338. [[CrossRef](#)]
50. Kongkaew, N.; Pruksakit, W.; Patumsawad, S. *Thermogravimetric Kinetic Analysis of the Pyrolysis of Rice Straw*; Elsevier B.V.: Amsterdam, The Netherlands, 2015; Volume 79.

51. Wnorowska, J.; Ciukaj, S.; Kalisz, S. Thermogravimetric Analysis of Solid Biofuels with Additive under Air Atmosphere. *Energies* **2021**, *14*, 2257. [[CrossRef](#)]
52. Florentino-Madiedo, L.; Vega, M.F.; Barriocanal, C. Evaluation of synergy during co-pyrolysis of torrefied sawdust, coal and paraffin. A kinetic and thermodynamic study. *Fuel* **2021**, *292*, 120305. [[CrossRef](#)]
53. Yuan, S.; Chen, H. Mathematical rules for synergistic, additive, and antagonistic effects of multi-drug combinations and their application in research and development of combinatorial drugs and special medical food combinations. *Food Sci. Hum. Wellness* **2019**, *8*, 136–141. [[CrossRef](#)]
54. El-Mahallawy, F.; El-Din Habik, S. *Fundamentals and Technology of Combustion*, 1st ed.; Elsevier Science: Cairo, Egypt, 2002; ISBN 978-0-08-044106-1.
55. Roberts, D.L. The inherent moisture content of South African Permian coals. *Int. J. Coal Geol.* **1991**, *17*, 297–311. [[CrossRef](#)]
56. Niu, S.; Chen, M.; Li, Y.; Song, J. Co-combustion characteristics of municipal sewage sludge and bituminous coal. *J. Therm. Anal. Calorim.* **2018**, *131*, 1821–1834. [[CrossRef](#)]
57. Zhou, Z.; Chen, L.; Guo, L.; Qian, B.; Wang, Z.; Cen, K. Computational modeling of oxy-coal combustion with intrinsic heterogeneous char reaction models. *Fuel Process. Technol.* **2017**, *161*, 169–181. [[CrossRef](#)]
58. Chen, P.; Zhang, L.; Huang, K. Kinetic Modeling of Coal Thermal Decomposition under Air Atmosphere. *Energy Fuels* **2016**, *30*, 5158–5166. [[CrossRef](#)]
59. Moran, M.; Shapiro, H. *Fundamentals of Engineering Thermodynamics*, 5th ed.; John Wiley & Sons: West Sussex, UK, 2006; ISBN 9781439833209.
60. Abdul Jameel, A.G.; Dahiphale, C.; Alquaity, A.B.S.S.; Zahid, U.; Jayanti, S. Numerical Simulation of Coal Combustion in a Tangential Pulverized Boiler: Effect of Burner Vertical Tilt Angle. *Arab. J. Sci. Eng.* **2021**, 1–14. [[CrossRef](#)]
61. Huang, Z.; Li, N. A comparative study of the pyrolysis and combustion characteristics of sodium-rich Zhundong coal in slow and rapid processes. *Energy Sci. Eng.* **2019**, *7*, 98–107. [[CrossRef](#)]
62. Sarroza, A.C.; Bennet, T.D.; Eastwick, C.; Liu, H. Characterising pulverised fuel ignition in a visual drop tube furnace by use of a high-speed imaging technique. *Fuel Process. Technol.* **2017**, *157*, 1–11. [[CrossRef](#)]
63. Tan, P.; Ma, L.; Xia, J.; Fang, Q.; Zhang, C.; Chen, G. Co-firing sludge in a pulverized coal-fired utility boiler: Combustion characteristics and economic impacts. *Energy* **2017**, *119*, 392–399. [[CrossRef](#)]